Available online at www.sciencedirect.com
ScienceDirect
International Journal of Heat and Mass Transfer 51 (2008) 5160–5174
International Journal of HEAT and MASS TRANSFER
www.elsevier.com/locate/ijhmt

A temperature fluctuation equation model dedicated to the computation of turbulent thermal layers in high Reynolds internal flows

Karine Truffin *, Adlène Benkenida

IFP, 1 à 4 av. du Bois-Préau, 92852 Rueil-Malmaison Cedex, France

Received 15 October 2007; received in revised form 14 February 2008
Available online 2 May 2008

Abstract

The paper deals with the modelling of temperature fluctuations in the fresh gases for the simulation of turbulent internal flows. For this purpose, a transport equation for the sensible enthalpy variance is treated. The proposed dynamic model for the scalar dissipation rate incorporates the effect of the turbulent Reynolds number. The wall closure is based on a non-isothermal formulation and accounts for the non-equilibrium state of the boundary layer. The developed models are implemented into the compressible code IFP-C3D. Results of the computations are successfully compared with experiments and DNS data for a slightly heated jet and moderate non-isothermal walls.

Keywords: Temperature fluctuation model; Wall model; Scalar dissipation

1. Introduction

Turbulent mixing in internal flows can be related to various phenomena, like mixing between fresh and burnt gases, evaporation, hot jet impacting on a wall or wall heat losses. Theses heterogeneities can have a strong impact on the combustion process and pollutant emissions in many industrial devices, like internal combustion engines. An accurate description of the turbulent fields is therefore required. The Reynolds Averaged Navier–Stokes (RANS) approach provides the mean fields. When the temporal or spatial fluctuations of a scalar are high, the mean value is not representative of the instantaneous value seen by the mesh cell and it is necessary to evaluate the statistical distribution of the quantity around its mean value. The modelling of the mixture fraction and its fluctuation has already been widely addressed [1–3]. However, the modelling of the temperature fluctuation in internal flows is still a work in progress.

A number of studies is devoted to the modelling of temperature fluctuations in turbulent homogeneous flows [4–6], in thermal mixing layers [6–9], in natural convection [10], in reactive flows [11–16] or in hypersonic flows [17,18]. A classical approach adopted in RANS calculations is to include a transport equation for the variance. The destruction term of the temperature variance ε_T is often closed using a simple algebraic closure, where a model constant C_0 must be adjusted [6,11,13,16]. Another approach is to model a transport equation for ε_T [7,19,20]. This method is especially adapted for the simulations of flows in simple geometries, for which the values of the model constants can be determined experimentally [5] of from Direct Numerical Simulation (DNS) data [21–23]. The temperature variance may also be strongly affected by the walls. The effect of isothermal walls, has actually widely been investigated in low-Reynolds number formulations [22,24–28], but is has almost never been addressed in high Reynolds [20]. In [20], the boundary conditions of the temperature variance

* Corresponding author. Tel.: +33 1 4752 5412; fax: +33 1 4752 7068.
E-mail address: karine.truffin@ifp.fr (K. Truffin).

0017-9310/$ - see front matter © 2008 Elsevier Ltd. All rights reserved.
doi:10.1016/j.ijheatmasstransfer.2008.02.042

Nomenclature

C_0 coefficient of the scalar dissipation rate
$C_f = \tau_w/(\frac{1}{2}\bar{\rho}\tilde{u}^2)$ Skin friction
$C_\mu = 0.09$ constant of the k–ε model
C_p specific heat at constant pressure
h_s mean sensible enthalpy
k turbulent kinetic energy
p pressure
P_h production of the sensible enthalpy variance
Pr Prandtl number
Pr_t turbulent Prandtl number
$q_w = -\lambda_w\left(\frac{\partial\widetilde{T}}{\partial y}\right)_{y=0}$ wall heat flux
$St = \frac{q_w}{\rho c_p(T_w - T_\infty)U_\infty}$ Stanton number
$T^+ = -(\widetilde{T} - T_w)/T_\tau$ dimensionless temperature
$T_\tau = q_w/(\rho_w C_p u_\tau)$ friction temperature
$u^+ = \tilde{u}/u_\tau$ dimensionless velocity
u_i velocity components
$u_\tau = \sqrt{\tau_w/\rho_w}$ shear velocity
v_T temperature variance
v_{h_s} sensible enthalpy variance
$y^+ = u_\tau y/\nu_w$ dimensionless distance
Y_k mass fraction of species k

Greek symbols
τ_{ij} viscous tensor
η^+ dimensionless distance
κ Von Kárman constant
λ Taylor microscale
λ_t turbulent conductivity
μ dynamic viscosity
μ_t turbulent viscosity
ν kinematic viscosity
ν_t eddy viscosity
ψ^+ dimensionless velocity
ρ mass density
$\rho^+ = \bar{\rho}/\rho_w$ dimensionless density
τ_h thermal time scale
τ_t turbulent integral time scale
$\tau_w = \mu_w(\frac{\partial\tilde{u}}{\partial y})_{y=0}$ wall shear stress
θ^+ dimensionless temperature
ε dissipation of the turbulent kinetic energy
ε_h scalar dissipation term of the sensible enthalpy variance
ξ isothermicity parameter

Subscripts
1 value in the first internal grid point
m bulk value
w wall value
$c1$ average value in the first internal computational cell

Superscripts
$\sim$ Favre average filtering,
$'$ fluctuation component associated to the Reynolds averaging
$''$ fluctuation component associated to the Favre averaging
$^+$ normalised by ρ, ν, u_τ and T_τ
$^-$ Reynolds average filtering

are formulated by assuming the equilibrium between its production and its dissipation. This assumption is not always realistic, especially in case of moving walls and perturbations by the turbulent motion of the external flow.

The aim of this study is to propose a simple model for the temperature variance in the fresh gases, specifically adapted to internal flow calculations, characterized by high Reynolds numbers and moderate temperature gradients (mixing with burnt gases, wall effects). The temperature variance v_T can be obtained either by transporting it directly [9,15,17,18,28–30] or by transporting the variance of another variable (energy, enthalpy [11,31] or sensible energy, sensible enthalpy [13]). Different types of variance transport equation were examined by Gerlinger [16] using the simulation of a supersonic hydrogen–air diffusion flame. In that case, it was found that the temperature variance equation provided best results, insofar as the variance was not considered as a passive scalar. The present paper focuses on non reactive flows. Moreover, it is a convenient choice to transport an extensive variable in a closed system. In the CFD code used in this work, the mean sensible enthalpy is treated to obtain the fresh gas temperature [32]. This study will therefore focus on the variance of the sensible enthalpy to be consistant with the mean transport equation. The temperature variance is then easily recovered as shown in Section 2. An algebraic closure is adopted for the closure of the scalar dissipation instead of modelling a transport equation, which suffers from a lack of closure models. However, the closure is improved thanks to a local evaluation of its constant on the base of the dynamic function of Donzis et al. [33]. Although it does not account for stratifications, it has been tested in a number of configurations presented here. A description of this model is given in Section 3. The combustion chamber walls in engines are characterized by consequential heat transfers [34], which are responsible for an increase in temperature fluctuations. The modelling of near wall phenomena is all the more difficult as they appear in very thin regions, requiring very fine resolution. In real engine simulations, a compromise must be found between computational costs and accuracy. For this reason, the convective heat transfers are modelled by wall-functions. This approach is simple, inexpensive and it can provide reasonable results under many flow conditions [35]. A summary of the law-of-the

wall principle and existing models can be found in [36]. The main interest of the present model is the introduction of a wall model to properly close the variance equation on isothermal walls. The originality of the model described in Section 4 holds two points:

- the non-equilibrium formulation in the boundary layer. First, the non-equilibrium assumption allows the skin friction to vanish immediately upon resticking. Second, the wall heat flux is proportional to the square root of the mean kinetic energy, which is consistent with measurements [37]. Third, the turbulent quantities are not estimated locally using the assumption *production = dissipation*, i.e. the formulation takes into account the effect of the external turbulent eddies interacting with the boundary layer.
- the anisotherm formulation LnKC [38–40]. This model was developed to account for strong temperature gradients that may be encountered near the walls in combustion chambers.

The resulting modelled variance equation is implemented into the IFP-C3D code [41,42] and applied in association with the k–ε model [43]. The validations are realised following two steps. First, computations of a slightly heated jet at high Reynolds number are compared with experiment [44,45]. This case is used to evaluate the behavior of the dynamic model for the scalar dissipation in inhomogeneous flows. In a second step, the variance behavior near the wall is validated using two configurations. The first one corresponds to a boundary layer formed on an isothermal wall. The calculations are compared with DNS results [46]. In the second one, the widely detailed experiment of a turbulent air flow injected into a heated pipe [47–50] has been chosen for the validation. The comparisons are realised for different longitudinal positions. The profiles of the production and destruction rates of the variance are also examined. These academic configurations do not exactly involve the whole condition encountered in real engines. Indeed the temperature difference between the wall and the inlet air is moderate. This is due to the lack of DNS and measurements data in realistic conditions (high Reynolds number, strong temperature gradients and temperature fluctuation). As a matter of fact, they allow to check the accuracy of the model in simple cases for moderate non-isothermal flows, where a number of rigorous and quantitative data are available.

2. Formulation of the variance equation

2.1. Equation for the mean sensible enthalpy

The present paper deals with Reynolds Average Navier–Stokes equations (RANS) for compressible flows. Each transported quantity f is defined by the Favre average formalism $\tilde{f}$, which is related to the Reynolds average $\bar{f}$ by

$$\tilde{f} = \frac{\overline{\rho f}}{\bar{\rho}}. \tag{1}$$

For each average, any quantity f may be split into mean and fluctuating component as

$$f = \bar{f} + f' \quad \text{and} \quad \bar{f}' = 0, \tag{2}$$

$$f = \tilde{f} + f'' \quad \text{and} \quad \tilde{f}'' = 0. \tag{3}$$

To obtain the temperature, a transport equation for the mean sensible enthalpy $\tilde{h}_s$ is solved [32]. In a multi-species flow, h_s is defined by

$$h_s = \sum_{k=1}^{N} Y_k h_{s,k} \quad \text{and} \quad h_{s,k} = \int_0^T C_{p,k}(\theta)\,\mathrm{d}\theta, \tag{4}$$

where Y_k is the mass fraction of species k, $h_{s,k}$ is its sensible enthalpy and $C_{p,k}$ its specific heat at constant pressure. To obtain the mean temperature from the sensible enthalpy value, we neglect temperature and species fluctuations in $C_{p,k}$ and the following approximation is required:

$$\overline{\rho Y_k \int_0^T C_{p,k}(\theta)\mathrm{d}\theta} \approx \bar{\rho}\widetilde{Y}_k \int_0^{\widetilde{T}} C_{p,k}(\theta)\mathrm{d}\theta, \tag{5}$$

where ρ is the mass density. The mean sensible enthalpy is then linked to the temperature by the following relation:

$$\tilde{h}_s \approx h_s(\widetilde{T}) = \int_0^{\widetilde{T}} C_p(\theta)\mathrm{d}\theta. \tag{6}$$

where C_p is the specific heat at constant pressure of the mixture ($C_p = \sum_{k=1}^{N} Y_k C_{p,k}$). Assuming unit Lewis number, the instantaneous transport equation of h_s is written following:

$$\frac{\partial \rho h_s}{\partial t} + \frac{\partial \rho u_i h_s}{\partial x_i} = \frac{\mathrm{d}p}{\mathrm{d}t} + \frac{\partial}{\partial x_i}\left(\frac{\mu}{Pr}\frac{\partial h_s}{\partial x_i}\right) + \tau_{ij}\frac{\partial u_i}{\partial x_j}, \tag{7}$$

where μ is the dynamic viscosity, Pr is the Prandtl number and u_i are the velocity components. $\mathrm{d}p/\mathrm{d}t$ is the dilatation term and $\tau_{ij}\partial u_i/\partial x_j$ is the viscous heat source term. The Reynolds average of Eq. (7) is modelled following [32]:

$$\frac{\partial \bar{\rho}\tilde{h}_s}{\partial t} + \frac{\partial \bar{\rho}\tilde{u}_i\tilde{h}_s}{\partial x_i} = \frac{\overline{\mathrm{d}p}}{\mathrm{d}t} + \frac{\partial}{\partial x_i}\left[\left(\frac{\mu}{Pr} + \frac{\mu_t}{Pr_t}\right)\frac{\partial \tilde{h}_s}{\partial x_i}\right] + \overline{\tau_{ij}\frac{\partial u_i}{\partial x_j}}, \tag{8}$$

where Pr_t is the turbulent Prandtl number and μ_t is the turbulent viscosity. μ_t is obtained from the k–ϵ model:

$$\mu_t = C_\mu \frac{\tilde{k}^2}{\tilde{\epsilon}}, \tag{9}$$

where $C_\mu = 0.09$.

2.2. Equation for the sensible enthalpy variance

The sensible enthalpy variance is defined by

$$v_{h_s} = \widetilde{h_s''^2} = \widetilde{h_s^2} - \tilde{h}_s^2. \tag{10}$$

The equation for v_{h_s} is obtained by deriving an equation for h_s^2 and another one for $\tilde{h}_s^2$. The first equation is obtained by

multiplying the transport equation of h_s (Eq. (7)) by $2h_s$ and then averaging. The second one is derived by multiplying Eq. (8) by $2\tilde{h}_s$. Finally, the variance equation takes the form:

$$\frac{\partial\bar{\rho}v_{h_s}}{\partial t}+\frac{\partial\bar{\rho}\tilde{u}_i v_{h_s}}{\partial x_i}=\underbrace{-\frac{\partial}{\partial x_i}(\bar{\rho}\widetilde{u_i''h_s''^2})}_{\mathrm{I}}\underbrace{-2\bar{\rho}\widetilde{u_i''h_s''}\frac{\partial\tilde{h}_s}{\partial x_i}}_{\mathrm{II}}\underbrace{+2\overline{h_s''\frac{\partial}{\partial x_i}\left(\frac{\mu}{Pr}\frac{h_s}{x_i}\right)}}_{\mathrm{III}}\underbrace{-2\overline{h_s''\frac{\mathrm{d}p}{\mathrm{d}t}}}_{\mathrm{IV}}\underbrace{+2\overline{h_s''\tau_{ij}\frac{\partial u_i}{\partial xij}}}_{\mathrm{V}}. \tag{11}$$

Eq. (11) contains several terms that need to be closed. For the turbulent transport (I) and the production (II) terms, a classical gradient assumption is usually adopted:

$$\bar{\rho}\widetilde{u_i''h_s''^2}=-\frac{\lambda_t}{C_p}\frac{\partial\widetilde{h_s''^2}}{\partial x_i}=-\frac{\mu_t}{Pr_t}\frac{\partial v_{h_s}}{\partial x_i}, \tag{12}$$

$$\bar{\rho}\widetilde{u_i''h_s''}\frac{\partial\tilde{h}_s}{\partial x_i}=-\frac{\mu_t}{Pr_t}\left(\frac{\partial\tilde{h}_s}{\partial x_i}\right)^2, \tag{13}$$

where λ_t is the turbulent conductivity. The diffusion term (III) is also written following:

$$\overline{2h_s''\frac{\partial}{\partial x_i}\left(\frac{\mu}{Pr}\frac{h_s}{x_i}\right)}=\underbrace{\frac{\partial}{\partial x_i}\left[\frac{\mu}{Pr}\left(\frac{\partial v_{h_s}}{\partial x_i}\right)\right]}_{D_h}\underbrace{-2\frac{\mu}{Pr}\left(\frac{\partial\widetilde{h_s''}}{\partial x_i}\right)^2}_{\chi_h}. \tag{14}$$

The first right hand side term D_h is the molecular diffusion of the enthalpy variance, while the second right hand side term χ_h represents the scalar dissipation. χ_h is mostly modelled using an algebraic closure [6,11,13,16]:

$$\chi_h=\bar{\rho}\tilde{\varepsilon}_h=-C_0\bar{\rho}v_{h_s}\frac{\tilde{\varepsilon}}{\tilde{k}}. \tag{15}$$

The dilatation term (IV) is difficult to model and it is often neglected [11]. In engines, the pressure variations can be assumed to be almost constant from cycle to cycle. The instantaneous variation $\mathrm{d}p/\mathrm{d}t$ is then close to its mean value: $\mathrm{d}p/\mathrm{d}t\approx\overline{\mathrm{d}p/\mathrm{d}t}$. The dilation term can then be approximated following:

$$-2\overline{h_s''\frac{\mathrm{d}p}{\mathrm{d}t}}\approx-2\overline{h_s''}\overline{\frac{\mathrm{d}p}{\mathrm{d}t}}. \tag{16}$$

If assuming the statistical mean of h_s'' is zero: $\overline{h_s''}\approx 0$, we can consider that the effect of the dilatation term is small compared to the other terms and for this reason it can eventually be neglected. The viscous dissipation term (V) is neglected at low Mach number due to the lack of possible modelling approach [11,16]. Finally, accounting for closures (12)–(16), we obtain the closed form of the variance equation:

$$\frac{\partial\bar{\rho}v_{h_s}}{\partial t}+\frac{\partial\bar{\rho}\tilde{u}_i v_{h_s}}{\partial x_i}=\underbrace{\frac{\partial}{\partial x_i}\left[\left(\frac{\mu}{Pr}+\frac{\mu_t}{Pr_t}\right)\left(\frac{\partial v_{h_s}}{\partial x_i}\right)\right]}_{D_h+D_{h,t}}\underbrace{+2\frac{\mu_t}{Pr_t}\frac{\partial\tilde{h}_s}{\partial x_i}\frac{\partial\tilde{h}_s}{\partial x_i}}_{P_h}\underbrace{-C_0\bar{\rho}v_{h_s}\frac{\tilde{\varepsilon}}{\tilde{k}}}_{\bar{\rho}\tilde{\varepsilon}_h}. \tag{17}$$

The temperature variance should then be determined from the sensible enthalpy variance value. Assuming small variations of C_p with the temperature and using Eq. (6) leads to

$$h_s-\tilde{h}_s=\int_{\widetilde{T}}^{T}C_p(\theta)\mathrm{d}\theta\approx C_p(\widetilde{T})\cdot(T-\widetilde{T}). \tag{18}$$

Using the relation $v_{h_s}=\widetilde{(h_s-\tilde{h}_s)^2}$ in Eq. (18) leads to $v_{h_s}=C_p^2(\widetilde{T})v_T$.

3. A dynamic model for the scalar dissipation

In the destruction term $\bar{\rho}\tilde{\varepsilon}_h$ of the sensible enthalpy variance in Eq. (17), the coefficient C_0 is the ratio of the turbulent integral time scale ($\tau_t=\tilde{k}/\tilde{\varepsilon}$) to the thermal time scale ($\tau_h=v_{h_s}/\tilde{\varepsilon}_h$) [51]: In the simplest algebraic closure, C_0 is usually set to 2. However, in grid-generated homogeneous turbulence [51,52], the measured value of C_0 can vary between 0.7 and 2.6. The examination of data obtained in non-isothermal shear flows [53] showed that C_0 could range between 1.7 and 2.9. Recently, Donzis et al. [33] noticed that the constant C_0 could take values from 1.2 up to 3 for moderate to large turbulent Reynolds numbers in homogeneous flows. For sufficiently large values only, the ratio τ_t/τ_h becomes a constant. When performing a calculation, the value of C_0 is not known "a priori", while it can vary in space and time. For this reason, the dynamic modelling proposed by Donzis et al. [33] is tested in this study. This model has been developed by compiling data of experiments and numerical simulations of homogeneous isotropic turbulent flows. An analytical solution was developed to reproduce the behavior of C_0 as a function of the turbulent Reynolds number associated to the Taylor microscale ($\lambda=\sqrt{10\nu k/\varepsilon}$). This Reynolds number is defined following:

$$Re_\lambda=\frac{\lambda\sqrt{2k/3}}{\nu}. \tag{19}$$

The resulting function $C_0(Re_\lambda)$ is written following:

$$C_0(Re_\lambda)=\frac{3\left(1+\sqrt{1+(31/Re_\lambda)^2}\right)}{1+\sqrt{1+(92/Re_\lambda)^2}}. \tag{20}$$

For very large values of Re_λ, C_0 tends to the asymptotic value 3. However for moderate and large values ($40<Re_\lambda<300$), C_0 varies between 1.7 and 3. The model is not accurate at small Reynolds number values ($Re_\lambda<40$). This is not a problem insofar as the turbulent Reynolds number remains quite high in automotive en-

gines, even though strong variations can be observed: typically Re_λ can vary between 50 and 300. It is noteworthy that this function has been developed for homogeneous flows. The situation in inhomogeneous flows and the role of viscosity in boundary layers have not been investigated yet. We propose in this paper simple verification of the dynamic model application.

4. Wall modelling

4.1. Preliminary

The term "law-of-the-wall" initially refers to the analytical relations providing the velocity and temperature profiles in the boundary layer. It is also currently used to designate the relations, that determine the wall shear stress τ_w and the wall heat flux q_w. For better clearness, the term"wall models" is employed here to designate all the relations for the mean and turbulent quantities at wall (k, ε and v_{h_s}). The principle of the wall model is shown in Fig. 1. The flow variables computed in the near wall cell) (point 1) are used together with the wall-functions to determine the wall fluxes and the turbulent quantities.

Usually, the assumption of quasi-isothermal near wall flow is required to formulate the wall models. Such an assumption is not valid in strongly anisotherm situations encountered in engines. The LnKC model [38,39,54] was developed to account for strong temperature gradients, generated mainly by combustion. It provides the wall laws and the wall fluxes formulations (shear stress, heat flux) that are needed to determine the thermodynamic quantities (mean longitudinal velocity and temperature) in the first mesh cell. This model is the basis of the present modelling for the temperature variance at wall. Indeed, the variance closure at wall has been constructed so as to be consistent with the boundary condition for the mean temperature.

The LnKC approach is briefly described in Section 4.2. Using adequate normalization, this model provides simplified expressions for the wall shear stress and for the wall heat flux. Starting from this model, closures for the production and dissipation terms of the sensible enthalpy variance are then proposed in Section 4.3.

4.2. Convective heat transfer formulation

In non-isothermal cases, the variations of the local density and viscosity can be important so that it is judicious to normalize the flow quantities using the local viscosity instead of the wall viscosity. The dimensionless variables are therefore defined following:

$$\mathrm{d}\eta^+ = \frac{v_w}{v}\,\mathrm{d}y^+, \quad \mathrm{d}\psi^+ = \rho^+\mathrm{d}u^+, \quad \mathrm{d}\theta^+ = \rho^+\mathrm{d}T^+, \tag{21}$$

where y^+, u^+ and T^+ are wall distance, the longitudinal velocity and the temperature normalised with the flow properties at wall. Using this formalism and the classical assumptions of the inner layer, the integration of the normalised momentum and enthalpy equations provide the law of the wall in the inertial boundary layer [38,40]:

$$\psi^+ = \kappa^{-1}\ln(\eta^+) + C_{\psi,0} \quad \text{and} \quad \theta^+ = Pr_t\kappa^{-1}\ln(\eta^+) + C_{\theta,0}, \tag{22}$$

where $\kappa = 0.41$ is the Von Kárman constant. $C_{\psi,0}$ and $C_{\theta,0}$ can be determined experimentally. Kays and Crawford [38] give: $C_{\psi,0} = 5.0$ and $C_{\theta,0} = 3.9$. The dimensionless distance at the first grid point η_1^+ is obtained by integrating Eq. (21). A simplification is introduced to relate η_1^+ to y_1^+:

$$\eta_1^+ = \int_0^{y_1^+} \frac{v_w}{v}\,\mathrm{d}y^+ \approx \frac{v_w}{v_1}y_1^+ = \frac{u_\tau y_1}{v_1}, \tag{23}$$

where v_1 is an average value of v between $y^+ = 0$ and $y^+ = y_1^+$. The purpose is now to established the relations linking ψ^+ to the wall shear stress τ_w and θ^+ to the wall heat flux q_w on the first grid point. It is then straightforward to estimate τ_w and q_w using the law-of-the-wall defined in Eq. (22). The wall shear stress τ_w is defined following:

$$\tau_w = \rho_w u_\tau^2. \tag{24}$$

The derivation of a non-equilibrium formulation for τ_w requires two estimations of u_τ: an estimation from turbulent kinetic energy when local equilibrium is reached $C_\mu^{1/4}\tilde{k}^{1/2}$ and the exact expression $u_\tau(\tilde{u}, \psi^+)$, which is obtained by integrating $\mathrm{d}\psi^+$ in Eq. (21):

$$\psi_1^+ = \int_0^{u_1^+} \frac{\bar{\rho}}{\rho_w}\,\mathrm{d}u^+ \approx \frac{\bar{\rho}_{c1}}{\rho_w}u_1^+ = \frac{\bar{\rho}_{c1}}{\rho_w}\frac{\tilde{u}_1}{u_\tau}, \tag{25}$$

where $\bar{\rho}_{c1}$ is an approximate of the average value in the cell and $\widetilde{u}_1$ is obtained on the first internal computational point. Finally, τ_w is expressed following:

$$\tau_w = \overline{\rho_{c1}}C_\mu^{1/4}\tilde{k}_1^{1/2}\frac{\widetilde{u}_1}{\psi_1^+}. \tag{26}$$

To determine the wall heat flux q_w, let introduce the isothermicity parameter $\xi = -T_\tau/T_w$ [36], where T_τ is the friction temperature. In piston engines, ξ can reach values larger than 0.5. Considering the pressure is constant in the inner layer, we can write:

$$\frac{\bar{\rho}}{\rho_w} = \frac{T_w}{\widetilde{T}} \quad \text{or} \quad \rho^+ = (1 + \xi T^+)^{-1}. \tag{27}$$

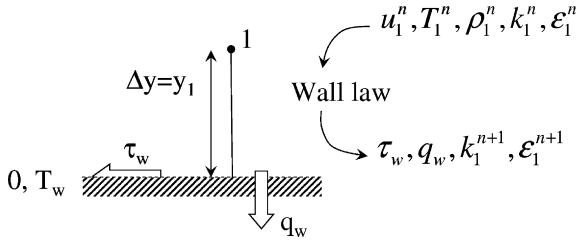

Fig. 1. Principle of the wall model.

Then integrating $\mathrm{d}\theta^+$ in Eq. (21) leads to

$$\theta^+ = \int_{\eta^+=0}^{\eta^+} \mathrm{d}\theta^+ = \int_{T^+=0}^{T^+} \frac{1}{1+\xi T^+}\,\mathrm{d}T^+ = \frac{1}{\xi}\ln(1+\xi T^+). \tag{28}$$

Using Eq. (28) and the relation $u_\tau = C_\mu^{1/4}\widetilde{k}^{1/2}$ leads to an expression for the heat flux q_w:

$$q_w = -\frac{\rho_w C_p C_\mu^{1/4} k_1^{1/2} T_w \ln(\widetilde{T}_1/T_w)}{\theta_1^+}, \tag{29}$$

where θ_1^+ is obtained with the wall law Eq. (22). Noteworthy, the asymptotic limit of Eq. (29) when $\widetilde{T}_1 \to T_w$ is the classical isothermal formulation of the wall heat flux:

$$q_w \underset{\widetilde{T}_1 \to T_w}{\longrightarrow} -\rho_w C_p C_\mu^{1/4} k_1^{1/2} \frac{\widetilde{T}_1 - T_w}{\theta_1^+}. \tag{30}$$

In the non-equilibrium approach, the production and dissipation terms of the turbulent kinetic energy $\widetilde{k}$ must be also determined by the law-of-the-wall. The mean production term $P_{k,c1}$ and the dissipation $\widetilde{\varepsilon}_{c1}$ in the wall cell are obtained by integrating their local values along the wall cell height [4,54]. Assuming that the sum of the laminar and turbulent shear stress is constant and that the relation $\varepsilon = C_\mu^{3/4}k^{3/2}/(\kappa y)$ is a correct estimation in the inner layer [55] the following estimations are obtained:

$$P_{k,c1} \approx \tau_w \frac{\widetilde{u}_1}{y_1} \quad \text{and} \quad \widetilde{\varepsilon}_{c1} \approx C_\mu^{3/4} k_1^{3/2} \frac{\psi_1^+}{y_1}. \tag{31}$$

Further details on the closure formulation can be found in [40,54].

4.3. Closure of the sensible enthalpy variance equation at walls: the LnKC $-v_h$ model

The purpose of this section is to propose modelling closures for the production and dissipation terms of the sensible enthalpy variance at walls. First, it is worth to notice that while the modelled wall shear stress is coupled with the computed turbulent kinetic energy, the modelled wall heat flux is independent of the temperature variance. The approach described below is therefore slightly different to the previous one for the turbulent kinetic energy. Our concern is to properly reproduce the behavior of the production and dissipation of the temperature fluctuation near the wall. First, assuming the heat flux is constant in the inertial layer allows to write:

$$P_h = 2\frac{\mu_t}{Pr_t}\left(\frac{\partial h_s}{\partial y}\right)^2 \approx 2\frac{Pr_t}{\rho \nu_t} q_w^2. \tag{32}$$

If local equilibrium is assumed between the production P_h (Eq. (32)) and the dissipation ε_h (Eq. (17)) of the sensible enthalpy variance ($P_h = \bar{\rho}\widetilde{\varepsilon}_h$), a simple boundary condition is obtained for v_{h_s}:

$$v_{h_s} = \frac{2Pr_t}{C_0 C_\mu \widetilde{k}}\left(\frac{q_w}{\bar{\rho}}\right)^2. \tag{33}$$

In the non-equilibrium approach, the production and dissipation terms of v_{h_s} must be determined by the law-of-the-wall. As the production and dissipation profiles in the inner layer can not be resolved, averaged values are modelled in the wall cell. For this purpose, the mean production and dissipation terms in the first computational cell are obtained by integrating their local values (Eq. (17)) along the wall cell height. First the integration of the production term requires attention:

$$P_{h,1} = \frac{1}{y_1}\int_0^{y_1} P_h\,\mathrm{d}y = \frac{1}{y_1}\left[\underbrace{\int_0^{y_c} P_h\,\mathrm{d}y}_{I_v} + \underbrace{\int_{y_c}^{y_1} P_h\,\mathrm{d}y}_{I_i}\right], \tag{34}$$

where I_v and I_i are the integral parts in the viscous sub-layer ($y < y_c$) and in the inertial sub-layer ($y > y_c$), respectively. The term I_v may be not negligible when the normalised wall distance is moderate ($\eta^+ \approx 50$) and the heat transfers are strong. For this reason, it can be at least roughly estimated. The production profile in the viscous sub-layer is difficult to estimate analytically. Nevertheless, it has been checked from DNS results [56] and measurements [49], that its average value is approximately equal to the average value in the region delimited by η_c^+ and $1.5\eta_c^+$: $I_v \approx \int_{y(\eta_c^+)}^{y(3\eta_c^+/2)} P_h\,\mathrm{d}y$. Then, using the local expressions $\nu_t = C_\mu k^2/\varepsilon$ and $\varepsilon = C_\mu^{3/4}k^{3/2}/(\kappa y)$ [55] leads to

$$P_{h,c1} = \frac{2Pr_t}{y_1}\frac{q_w^2}{C_\mu^{1/4}\widetilde{k}_1^{1/2}}\left[\int_{y_c}^{3y_c/2}\frac{1}{\kappa y}\,\mathrm{d}y + \int_{y_c}^{y_1}\frac{1}{\kappa y}\,\mathrm{d}y\right]. \tag{35}$$

The correlation between density and wall distance is unknown in the inner layer, so that the following approximation is obtained through a simple change of variables:

$$P_{h,c1} = \frac{2Pr_t}{\overline{\rho_1} y_1}\frac{q_w^2}{C_\mu^{1/4}\widetilde{k}_1^{1/2}}\left[\int_{\eta_c^+}^{3\eta_c^+/2}\frac{1}{\kappa\eta^+}\,\mathrm{d}\eta^+ + \int_{\eta_c^+}^{\eta_1^+}\frac{1}{\kappa\eta^+}\,\mathrm{d}\eta^+\right]. \tag{36}$$

Finally, the integration gives:

$$P_{h,c1} = \frac{2}{\bar{\rho}}\frac{Pr_t q_w^2}{C_\mu^{1/4}\widetilde{k}_1^{1/2}}\frac{1}{\kappa y_1}\ln(1.5\eta_1^+/\eta_c^+), \tag{37}$$

where the value of η_c^+ is set to 13.2 [38,54]. The integration of the dissipation term is realised by an analogy with the production. The standard algebraic closure is assumed to be proper estimation of the local variance dissipation in the inertial layer. The dissipation coefficient C_0 is generally found to be almost constant and close to 1.0 in wall shear layers [20,23,57,58]. For this reason, C_0 is set to 1.0 in the first grid point.

$$\widetilde{\varepsilon}_{h,c1} = \frac{1}{y_1}\int_0^{y_1} C_0 \frac{\tilde{\varepsilon}}{\tilde{k}} v_{h_s}\,\mathrm{d}y = \frac{C_0}{y_1}\left[\int_{y_c}^{3y_c/2} \frac{\tilde{\varepsilon}}{\tilde{k}} v_{h_s}\,\mathrm{d}y + \int_{y_c}^{y_1} \frac{\tilde{\varepsilon}}{\tilde{k}} v_{h_s}\,\mathrm{d}y\right]. \tag{38}$$

Using $\varepsilon = C_\mu^{3/4}k^{3/2}/(\kappa y)$, the following approximation is obtained:

$$\tilde{\varepsilon}_{h,c1} = \frac{C_0 C_\mu^{3/4}\tilde{k}_1^{3/2} v_{h_{s,1}}}{y_1}\left[\int_{\eta_c^+}^{3\eta_c^+/2} \frac{1}{\kappa\eta^+}\,\mathrm{d}\eta^+ + \int_{\eta_c^+}^{\eta_1} \frac{1}{\kappa\eta^+}\,\mathrm{d}\eta^+\right], \tag{39}$$

where $\tilde{k}_1$ and $v_{h_{s,1}}$ are mean values of the turbulent kinetic energy and of the sensible enthalpy variance in the wall cell obtained from the previous iteration. Finally, the integration gives:

$$\tilde{\varepsilon}_{h,c1} = \frac{C_0 C_\mu^{3/4}\tilde{k}_1^{3/2} v_{h_{s,1}}}{\kappa y_1}\ln(1.5\eta_1^+/\eta_c^+). \tag{40}$$

It is easy to check that the resulting models for $\tilde{\varepsilon}_{h,c1}$ and $P_{h,c1}$ coincide with the equilibrium state when one writes: $P_{h,c1} = \bar{\rho}\widetilde{\varepsilon}_{h,c1}$:

$$\frac{2}{\bar{\rho}}\frac{Pr_t q_w^2}{C_\mu^{1/4}\tilde{k}_1^{1/2}}\frac{\ln(1.5\eta_1^+/\eta_c^+)}{\kappa y_1} = C_0 C_\mu^{3/4}\tilde{k}_1^{3/2} v_{h_{s,1}}\frac{\ln(1.5\eta_1^+/\eta_c^+)}{\kappa y_1}, \tag{41}$$

which is similar to the equilibrium relation (33).

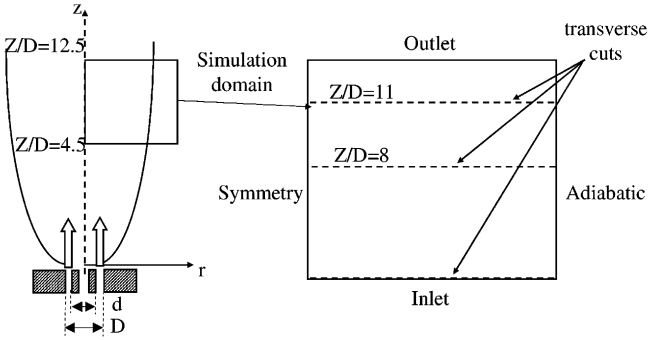

Fig. 2. Sketch and boundary conditions for the heated round jet.

5. Validations in thermal mixing layers

The thermal mixing layer is of interest because it involves mean advection, molecular and turbulent mixing which must be accounted for in the temperature variance modelling. Besides, the mixing zones between the turbulent flows of different temperatures show temperature gradients and fluctuations.

Three-dimensional simulations are performed using the compressible IFP-C3D code [41,42]. This code solves the unsteady Navier–Stokes equations using a finite volume method. The temporal integration is achieved using implicit method and time splitting decomposition [59].

5.1. Comparison with experiments

Experiments are carried out in an axisymmetric vertical turbulent air jet issuing from an annular nozzle [44,45]. The inside diameter is $d = 18.2$ mm and the outside diameter is $D = 25.3$ mm (Fig. 2). The annular flow is slightly heated by means of an electrical resistance. The flow rate is 15 m^3 h^{-1} and the maximum difference of temperature between the jet and the ambient temperature is 22 K. The Reynolds number based on the outside diameter and on the bulk velocity is $Re = 22,600$. The mean longitudinal velocity was measured with a special Pitot tube while the mean temperature was measured with thermocouples (0.15 mm diameter Chromel–Chromel–Constantan) and cold wires ($d = 0.63$ μm, Platinum). The temperature fluctuations were measured with the cold wire. The error on $\sqrt{v_T}$ is about 10%. Two series of temperature measurements were realised: the first one in 1981 [44] and the second one in 1988 [45]. Both of them are used for comparisons.

To simulate the experimental jet, the computational domain was chosen to be identical to previous numerical studies [6,45]. The calculation domain begins at $z/D = 4.5$ and extends to $z/D = 12.5$. The computational domain and boundary conditions are presented in Fig. 2. The corresponding physical size of the domain is 20 × 20 cm in the

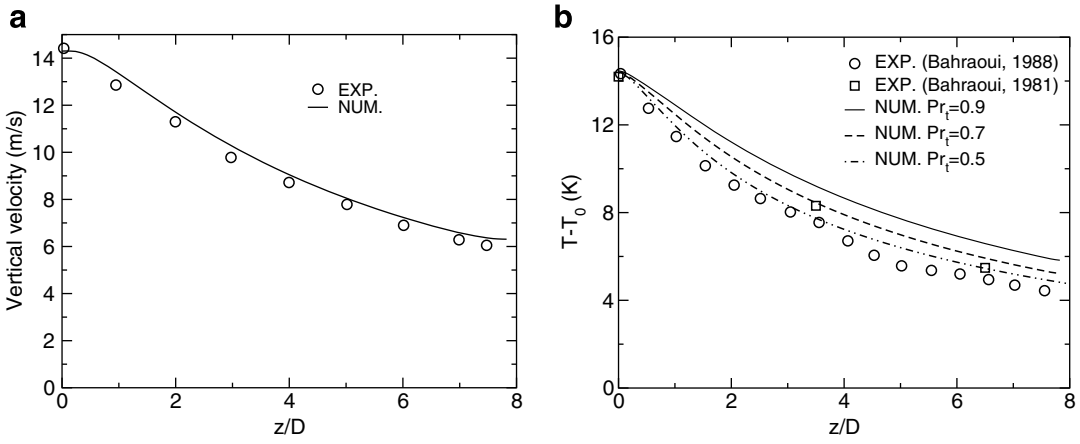

Fig. 3. Axial profiles: (a) mean vertical velocity; (b) mean temperature.

(r,z) plane. The number of grid points is $65 \times 3 \times 77$. Uniform grid spacing is used for the longitudinal direction. A hyperbolic tangent function is adopted to refine the grid in the thermal mixing layer, such as $\Delta y_{\min} = 0.7$ mm. The experimental results at $z/D = 4.5$ were used as inlet conditions for the simulation. The comparisons are realised along the central axis and along two radial axes positioned at $z/D = 8$ and $z/D = 11$, respectively (see Fig. 2). Special attention is paid to the value of the turbulent Prandtl number. In shear flows, values can range within 0.5 and 1.0, as found in the literature [60–62]. For this reason, different values of the turbulent Prandtl number were tested ($Pr_t = 0.5, 0.7$ and 0.9). Figs. 3 and 4a–d show comparisons of the mean quantities. The axial decay of velocity in Fig. 3a and the width of the dynamic mixing layer in Fig. 4a and b are accurately reproduced. The mean temperature profiles are compared in Figs. 3 and 4b–d. Although the maximum temperature along the symmetry axis is slightly overestimated (Fig. 3b), the width and slope of the transverse profile are correctly predicted when using

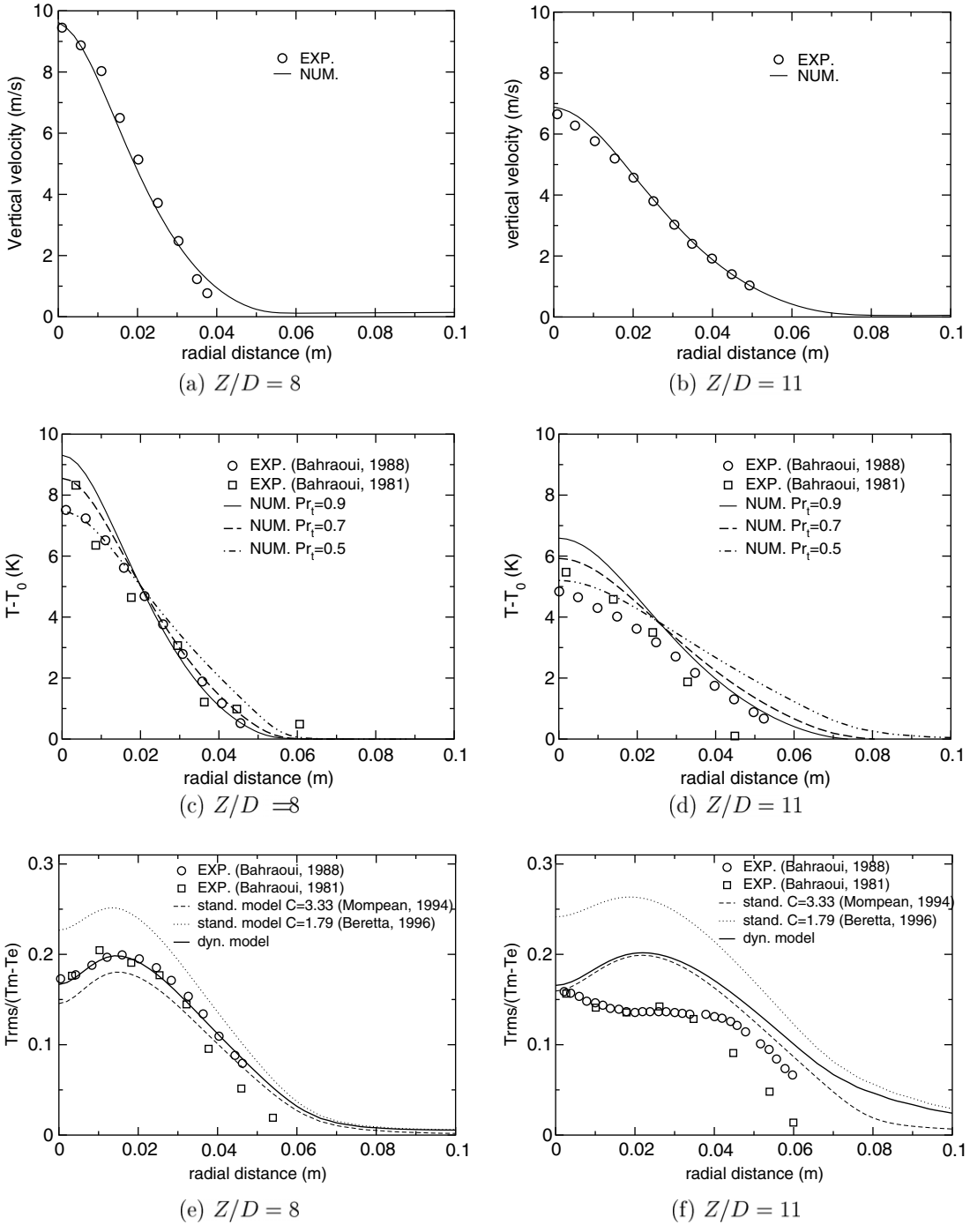

Fig. 4. Transverse profiles: (a) and (b) mean vertical velocity; (c) and (d) mean temperature; (e) and (f) rms temperature fluctuation profiles.

$Pr_t = 0.7$. The temperature variance is now examined. For this purpose, three simulations were performed with different values of the scalar dissipation coefficient C_0. For two of them, a fixed value of C_0 was chosen: $C_0 = 1.79$ as proposed in [13], $C_0 = 3.33$ as used by Mompean [6], who computed the same flow. In the third simulation, the dynamic model (Eq. (20)) was used. The Reynolds number associated to the Taylor field is somewhat high $Re_\lambda \approx 150$. This value lies within the domain of validity of the dynamic model. The visualization of the dynamic function in a 2D field (Fig. 5) shows that the computed C_0 value reaches a maximum value in the air jet, where the velocity is high ($C_0 \approx 2.9$), while it is minimum in the outer region. The normalised temperature fluctuations in the two cross-sections are plotted in Fig. 4e and f. The level and shape are quite well predicted with the dynamic model, compared to the standard model. Nevertheless, discrepancies are observed at $z/D = 11$. This may be due to the slight overestimation of the temperature slope near the symmetry axis.

6. Validations in thermal boundary layers developing on isothermal walls

Many studies can be found in the literature dealing with direct numerical simulations of a thermal boundary layer [23,46,56,63–65], but only a very few of them were realised with high Reynolds number [23,46]. Similarly, only a limited amount of experimental studies have been done to measure the temperature field and its fluctuation in turbulent wall boundary layers [47,66,67]. The validation of the wall model for the temperature variance is conducted using the DNS results of Kong et al. [46] for a turbulent thermal boundary evolving on a flat plate and the well detailed experiment of Hishida and Nagano [47–50] for a heated pipe. As explained in the introduction, these academic tests are not exactly representative of the conditions encountered in the combustion chambers of internal engines. However, the amount of reference data and the accuracy of results required for the model validation are not available for the moment in more complex or realistic configurations.

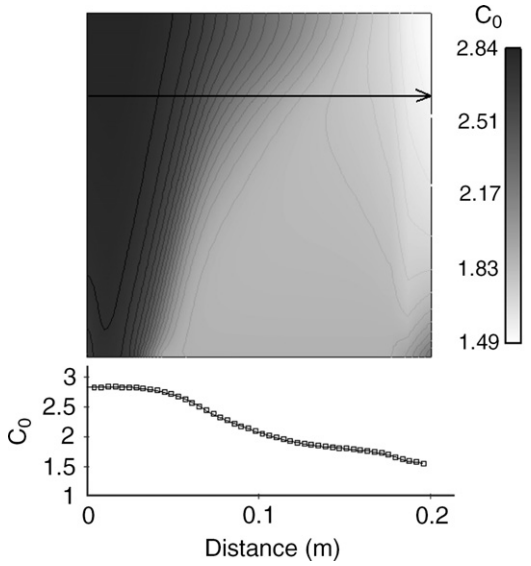

Fig. 5. Mean field of the scalar dissipation coefficient $C_0(Re_\lambda)$.

6.1. Comparison with DNS results

The Reynolds number based on the free stream velocity and on the half height L of the channel is 9510, which corresponds to a Reynolds number of 3.8×10^4, based on the hydraulic diameter $D_L = 4L$. The corresponding physical size of the domain is 20×2 cm in the (x, y) plane (see scheme in [46]). The simulation runs in a computational domain with $101 \times 22 \times 3$ grid points. Uniform grid spacing is used for the longitudinal direction. A hyperbolic tangent function is used to refine grids near the wall in the normal direction, such as $\Delta y_{min} = 0.8$ mm, which corresponds to $y_1^+ \approx 35$. The boundary layer develops from the inlet, such that at $x = 0$, the momentum thickness of the boundary layer $\delta_2 = 0$ and the thermal thickness $\Delta_2 = 0$. In the inlet, the hydrodynamic field is determined by the axial velocity $U = 15$ m s^{-1}, the turbulent kinetic energy $k = 0.1$ m^2 s^{-2} and its dissipation rate $\varepsilon = (u'^2)^{3/2}/l_t$ with $l_t = 6.67$ mm. For the thermal field, the inlet temperature is $T = 310$ K. There is no temperature fluctuation at inlet. The atmospheric pressure is imposed in the outlet. The wall is located at $y = 0$ and the wall temperature is $T_w = 373$ K. Symmetrical conditions are imposed on the opposite face. Periodic boundary conditions are employed on the faces normal to the z-direction. The turbulent Prandtl number is set to 0.8 according to the DNS results [46].

In addition to thermal and dynamic profiles, the simulation should match the prediction of wall fluxes. The validation can be achieved by comparing the computed heat transfers and skin frictions with the DNS data and empirical correlations (see Appendix A in [46]). For these comparisons, two non-dimensioned coefficients are examined: the skin friction (C_f) and the Stanton number (St). The evolution of the skin friction coefficient is shown in Fig. 6a as a function of the Reynolds number associated to the momentum thickness Re_{δ_2} (Eq. (A2) in [46]). The present result is in excellent agreement with the DNS and the empirical relation (Eq. (A1) in [46]). Fig. 6b shows the variation of the Stanton number as a function of the Reynolds number associated to the enthalpy thickness (Eqs. (A7) and (A10) in [46]). The numerical result agrees well with the DNS and the empirical relation (Eq. (A8) in [46]). Now, the mean flow field can be regarded. The mean velocity and temperature behavior near the isothermal wall are treated by the LnKC model described in Section 4.2. It is first necessary to check the mean flow computation in the boundary layer before validating the temperature fluctuation model. The transverse dynamic profiles are presented in Fig. 7 in terms of axial velocity (a) and turbulent kinetic energy (b). The velocity is quite

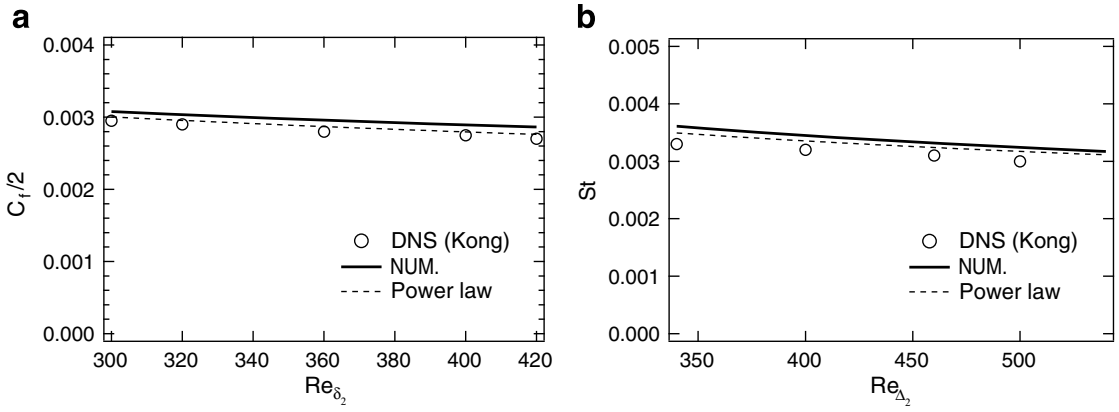

Fig. 6. Longitudinal profiles: (a) skin friction coefficient; (b) Stanton number. Symbols: DNS [46], solid lines: LnKC model [54,40], dashed lines: power-law approximations (Eqs. (A1) and (A8) in [46]).

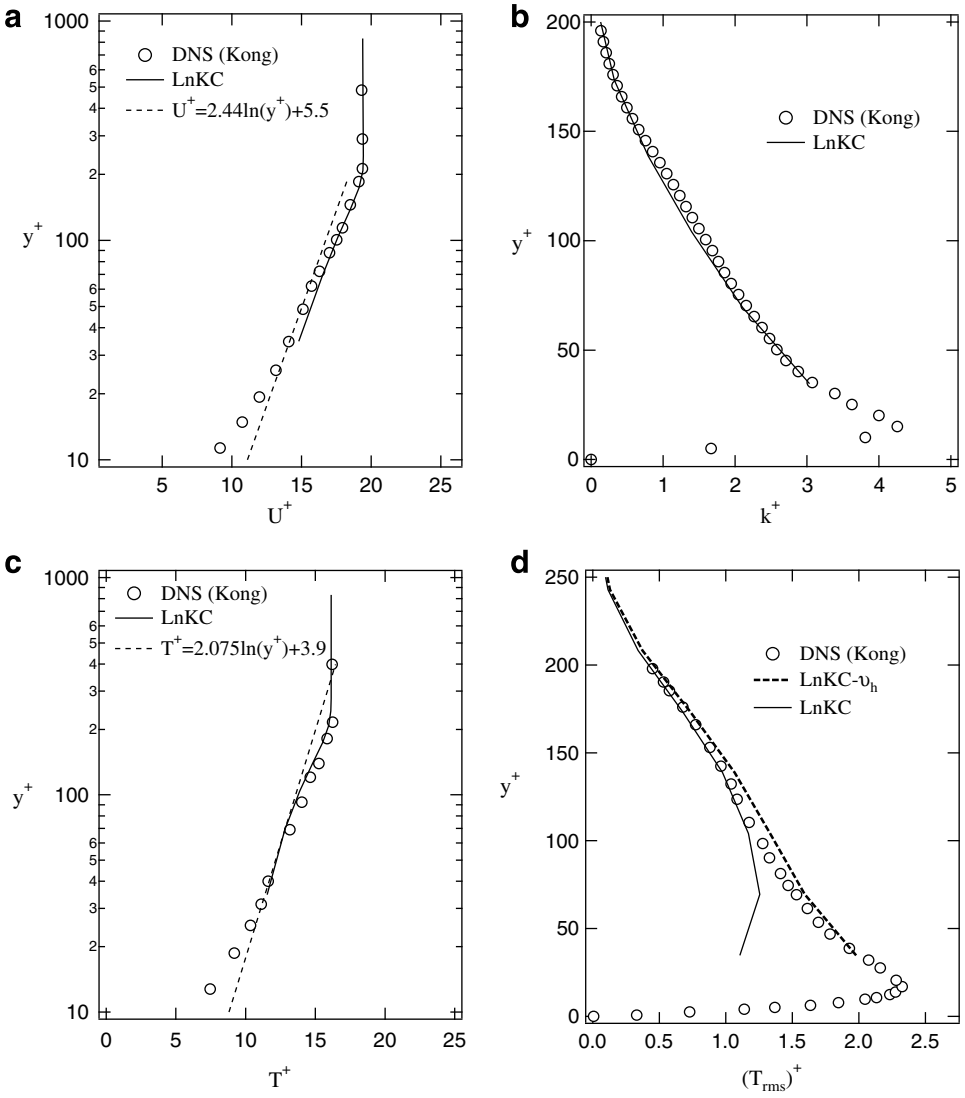

Fig. 7. Transverse profiles at $Re_{\delta_2} = 400$ and $Re_{\Delta_2} = 493$: (a) mean axial velocity; (b) turbulent kinetic energy; (c) mean temperature; (d) rms temperature fluctuation. Symbols: DNS [46]; dotted-dashed lines: logarithmic law [46]; solid lines: numerical results obtained with the LnKC model [54,40], bold dashed lines: numerical results obtained with the LnKC $-v_h$ model.

well predicted compared to the DNS and the logarithmic law. The transverse profile of the turbulent kinetic energy is also well reproduced. The mean temperature presented in Fig. 7c is correctly predicted, compared to the DNS and to the logarithmic law. The main flow variables being checked, we can now validate the computed temperature fluctuation plotted in Fig. 7d. Heat fluxes at wall induce temperature fluctuations in the logarithmic region. To check this, a computation was performed with the LnKC model without applying the wall closure for the sensible

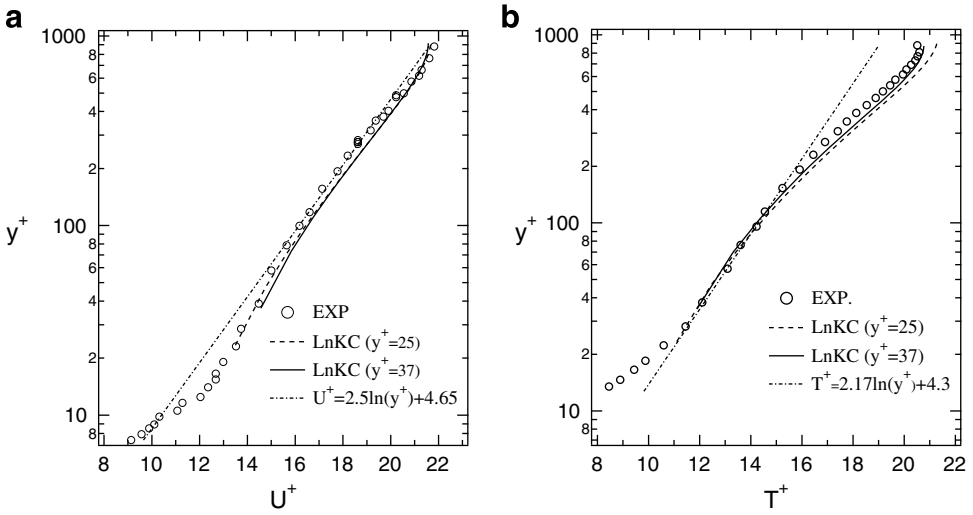

Fig. 8. Normalised transverse profiles at $x/D = 39.89$: (a) mean longitudinal velocity; (b) mean temperature.

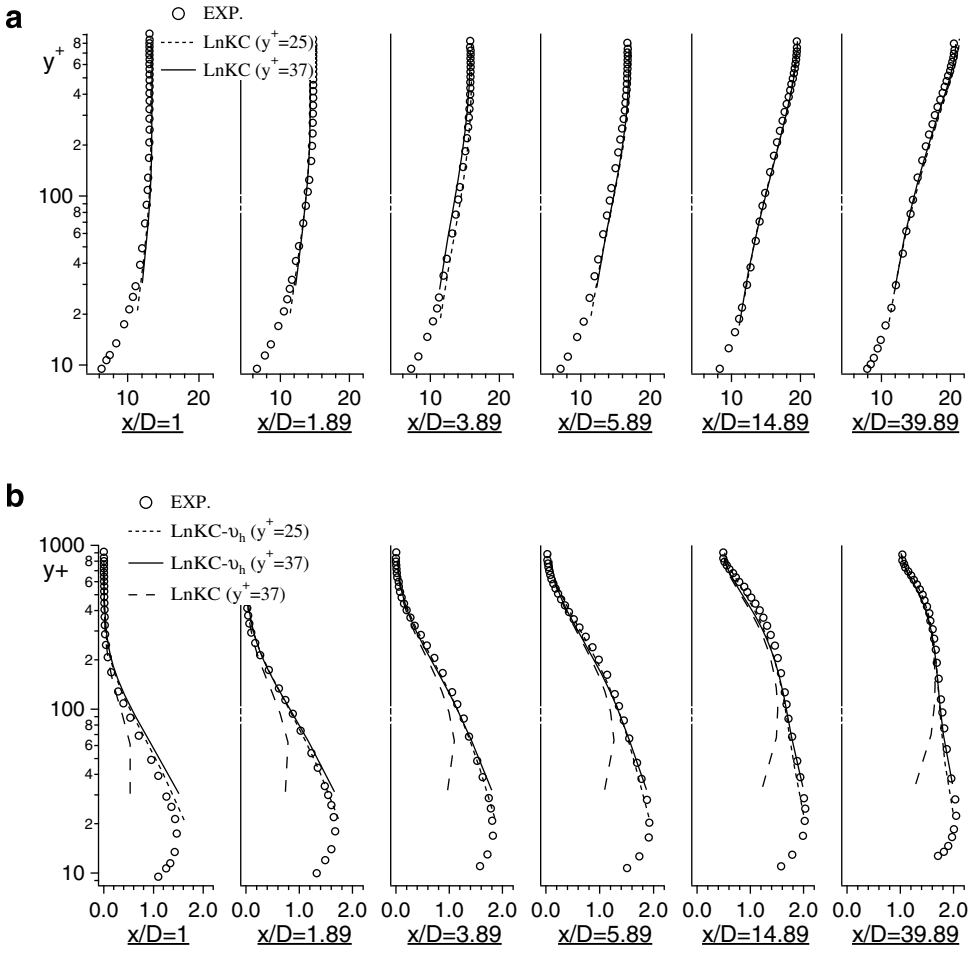

Fig. 9. Transverse profiles for different longitudinal locations: (a) mean normalised temperature T^+; (b) normalised profiles of the rms temperature fluctuation $\sqrt{v_T^+}$.

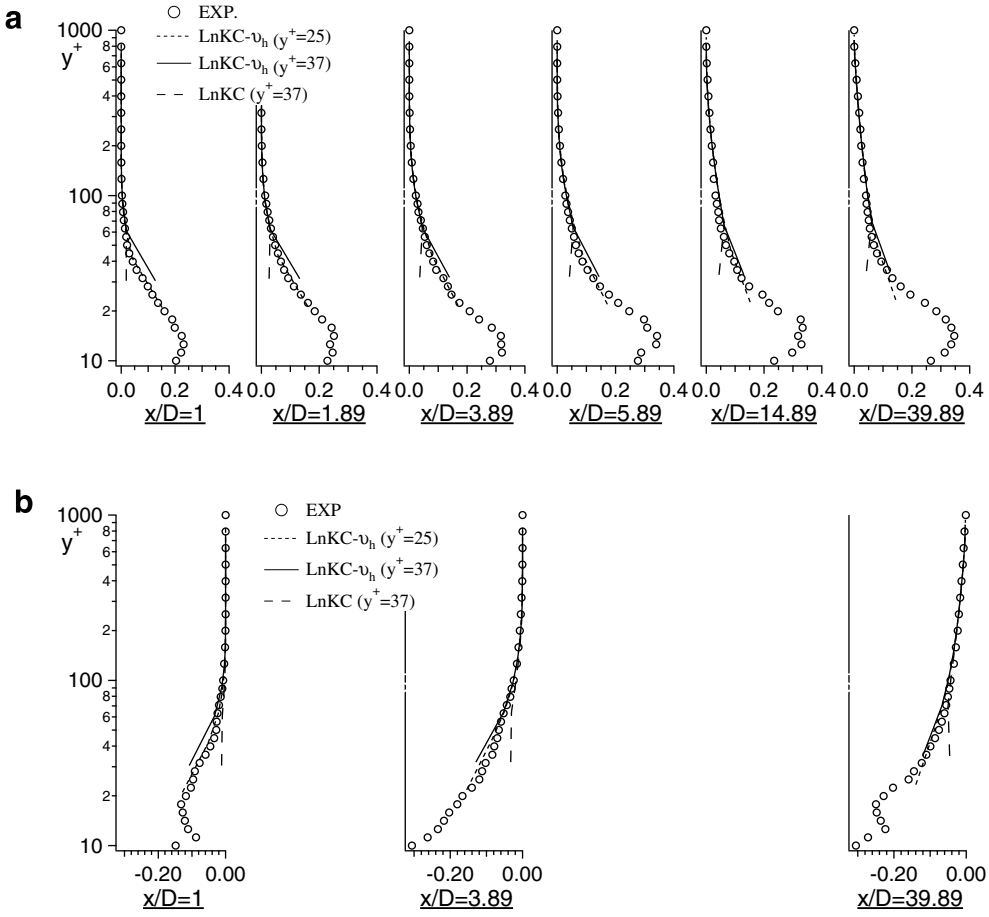

Fig. 10. Transverse profiles for different longitudinal locations: (a) normalised production rate of the temperature variance P_T^+ (Eq. (37)); (b) normalised destruction rate of the temperature variance ε_T^+ ((Eq. (40)).

enthalpy variance v_h. In that case, the production and dissipation terms are determined locally from their expressions in Eq. (17). The result is then compared with the LnKC $-v_h$ model, that includes appropriate wall closure for v_h (Eqs. (37) and (40)). Without wall model for the enthalpy variance, the temperature fluctuation level decreases near the wall. Using the wall model, the temperature fluctuation behavior is very close to the reference one.

6.2. Comparison with experiments

The test section was constructed from a brass tube with $D = 45.68$ mm in diameter and 2079 mm($45.5D$) in length. The section was heated with a uniform wall temperature $T_w = 373$ K. An unheated pipe upstream of the test section with $127D$ length. Simultaneous measurements of velocity components and temperature were realised with a three-wire probe technique (two hot wires together with a cold one). Details of the experimental apparatus and procedure are given in [49,50]. Numerical investigations and simulations of this configuration have also been performed [28,68] to validate low-Reynolds formulations, for which near wall turbulence statistics is resolved. However, the Reynolds number based on the tube diameter and inlet axial velocity ($U_0 = 17$ m s^{-1}) is $Re = 40,000$. Consequently, this is a suitable validation test for the present wall model. The axisymmetric computational domain corresponds to a section of the heated pipe. Two uniform grid spacing were used for the simulations, $322 \times 26 \times 3$ grid points and $322 \times 42 \times 3$ grid points, such that the normalised wall distance approximates $y_1^+ \approx 37$ and $y_1^+ \approx 25$, respectively. The simulation of the turbulent air flow in the unheated pipe was performed to obtain the dynamic inlet conditions of the heated pipe. The inlet temperature is $T_{inlet} = 314$ K. The turbulent Prandtl number is set to 1.0 according to the experiment [50]. A simulation without wall model for the enthalpy variance was also performed for comparison.

The comparisons are realised at six cross-sections ($1 \leqslant x/D \leqslant 39.89$) for the axial velocity, the temperature and its fluctuation. The behavior of the modelled production and dissipation of the temperature variance are also quantitatively validated. The experimental data are available on the DATHET web site.[1] For the normalization, physical properties of fluid are evaluated at the film temperature $T_f = (T_w + T_m)/2$, where T_m is the bulk temperature. The mean velocity and the mean temperature obtained at $x/D = 39.89$ (Fig. 8) agree well with the mea-

[1] http://www.jsme/or.jp/ted/HTDB/Forced/Wall/fw_pi006.csv.

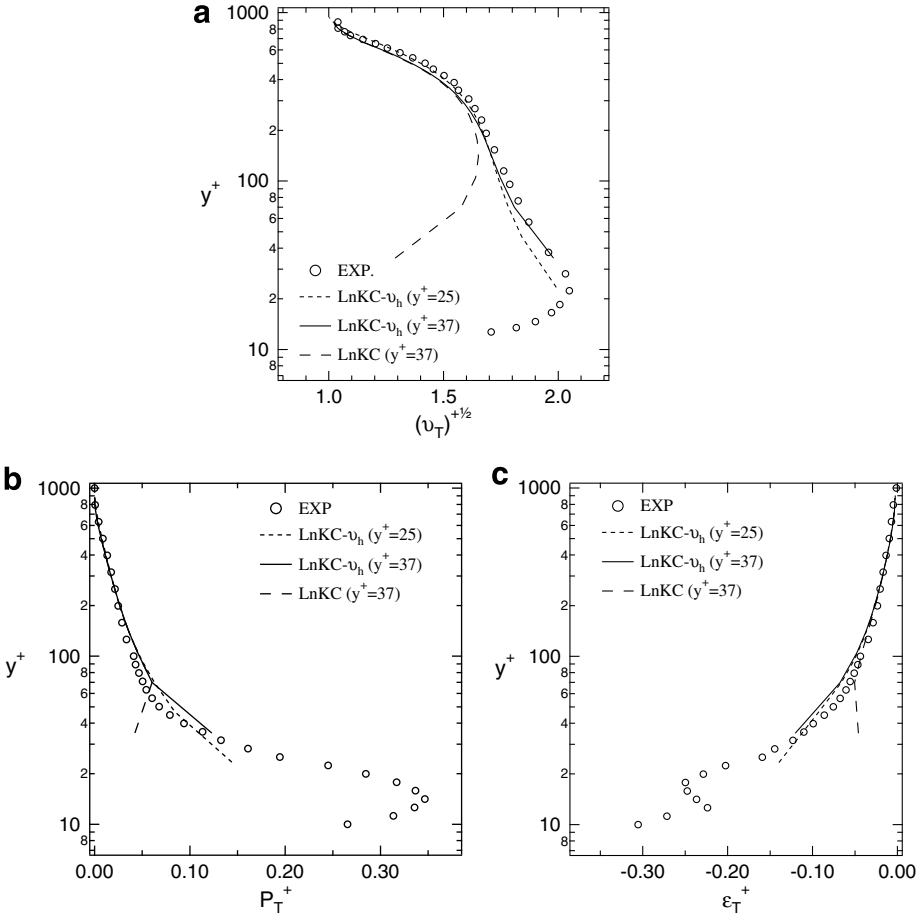

Fig. 11. Normalised transverse profiles at $x/D = 39.89$: (a) rms temperature fluctuation; (b) production rate of the temperature variance; (c) destruction rate of the temperature variance.

surements and the logarithmic law [47]. Considering the characteristics of the boundary layer, the region $30 < y^+ < 100$ refers to the inertial sub-layer. Consequently, the first grid point of the coarsest mesh is located in the inertial sub-layer ($y^+ = 37$), while the first grid point of the finest mesh ($y^+ = 25$) is located at the bottom limit of the inertial sub-layer. As seen in Fig. 9a, the logarithmic temperature profile in the fully turbulent region is not established even at $x/D = 5.89$ and the fully developed state is not reached before $x/D = 15$. However, the evolution of the temperature far from the wall is quite well predicted. The rms temperature fluctuation is shown in Fig. 9b. The effect of the wall model can be first evaluated by comparing the results obtained without and with the wall model for the enthalpy variance. Using the wall model LnKC $-v_h$, the temperature fluctuation shape and level are correctly predicted. Discrepancies are visible only in the undeveloped region at the beginning of the heated section. The profiles obtained with the finest mesh are also in very good agreement with the measurements. The modelling of the production and destruction rates of the temperature variance is accurate for both meshes (Fig. 10a and b, respectively). For a better visualization, the normalised profiles $\sqrt{v_T^+}$, P_T^+ and ε_T^+ at $x/D = 39.89$ are plotted in Fig. 11. The near wall values computed with the finest mesh are slightly underestimated. This result is not surprising insofar as the values of the production and of the dissipation obtained at the first calculation point (cell centered) should correspond to the mean integrated values of the profiles along the cell height. As explained in Section 4.3, the modelled production and dissipation terms are estimated through the integration of their local profiles (between $y = 0$ and $y = y_1$).

7. Conclusion

The modelling of temperature fluctuations in the fresh gases of high Reynolds internal flows, is investigated in this paper. For this purpose, a transport equation for the sensible enthalpy variance is treated. First, the recent study of Donzis et al. [33] has been exploited to develop a dynamic model for the scalar dissipation rate. This model incorporates the effect of the turbulent Reynolds number, which can vary considerably in engines. It is an alternative to the standard algebraic closure, which needs a constant to be fixed depending on the configuration and to a transport equation for the scalar dissipation, which implies further computing and modelling efforts. Mainly, near wall closure

is proposed for the transport equation of the sensible enthalpy variance. This closure is based on an anisothermal formulation for the mean quantities, the model LnKC [40,54], which allows to account for strong temperature gradients. Moreover, the proposed modelling accounts for the non-equilibrium state of the turbulent boundary layer, when interactions with the external flow occur.

In a second part, these models are validated using DNS results and measurements in simple steady configurations. The validation on simple test cases (weakly heated jet, flat plate and heated pipe) is a necessary step before computing more complex geometries. The simulations of thermal layers show quantitatively excellent agreements with the data [45]. Moreover, the accuracy of the dynamic model as a function of the Reynolds number is verified. Next, the simulations of turbulent thermal boundary layers allow to validate the wall model. The results exhibit very accurate behavior, especially comparisons of the temperature variance, its production and its dissipation are excellent. It must be pointed out that this study is a first step towards the prediction of temperature fluctuations generated by turbulence, heat transfers, thermal segregation and cycle-to-cycle variations in real internal engines. The present model has been validated only for moderate non-isothermal flows. The next step will be the examination of the model accuracy in a real engine configuration. Moreover, preliminary computations of auto-ignition have been performed. The auto-ignition model is based on the thermodynamic properties of the fresh gases. The coupling with the temperature fluctuation in the fresh gases, generated by wall heat losses, have already shown strong impact on the ignition process. Most importantly, a significant modification of the combustion process has been observed even though auto-ignition starts far from the wall in the middle chamber. These results seem to confirm some recent experimental observations [69]. These very promising tests demonstrate that a proper modelling of the temperature variance can be an essential requirement to reproduce the combustion event. The model validation in real internal engine and the coupling with combustion will be the purpose of a future paper.

Acknowledgements

This work was partially funded by the ANR PREDIT French program and by Renault SA. The authors would like to thank Dr. Christian Angelberger (IFP) and Dr. Olivier Colin (Air Liquide) for fruitful discussions.

References

[1] J. Reveillon, L. Vervisch, Accounting for spray vaporization in non-premixed turbulent combustion modeling: a single droplet model (sdm), Combust. Flame 121 (2000) 75–99.
[2] F. Demoulin, R. Borghi, Modeling of turbulent spray combustion with application to diesel like experiments, Combust. Flame 129 (2002) 281–293.
[3] O. Colin, A. Benkenida, A new scalar fluctuation model to predict mixing in evaporating TXO-phase flows, Combust. Flame 134 (2003) 207–227.
[4] B. Launder, D. Spalding, Further results on the thermal mixing layer downstream of a turbulence grid, Comput. Methods Appl. Mech. Eng. 3 (1974) 269–289.
[5] G. Newman, B. Launder, J. Lumley, Modeling the behaviour of homogeneous scalar turbulence, J. Fluid Mech. 111 (1981) 217–232.
[6] G. Mompean, Three-equation turbulence model for prediction of the mean square temperature variance in grid-generated flows and round jets, Int. J. Heat Mass Transfer 37 (7) (1994) 1165–1172.
[7] S. Elghobashi, B. Launder, Turbulent time scales and the dissipation rate of temperature variance in the thermal mixing layer, Phys. Fluids 26 (1983) 2415–2419.
[8] M. Gibson, W. Jones, V. Kanellopoulos, Turbulent temperature mixing layer – measurements and modelling, in: J.C. Andre et al. (Eds.), Turbulent Shear Flows, vol. 6, Springer-Verlag, Berlin, Heidelberg, 1989, pp. 119–129.
[9] T. Muramatsu, H. Ninokata, Intensity evaluation of the temperature fluctuations related TP thermal striping phenomena using the algebraic stress turbulence model, in: Proceedings of the ANS Winter Meeting, San Francisco, USA, 1991, pp. 156–162.
[10] I. Otić, G. Grötzbach, M. Wörner, Analysis and modelling of the temperature variance equation in turbulent natural convection for low-Prandtl-number fluids, J. Fluid Mech. 525 (2005) 237–261.
[11] R. Gaffney, J. White, S. Girimaji, J. Drummond, Modeling turbulence chemistry interactions using assumed pdf methods, in: Proceedings of the 30th AIAA Aerospace Sciences Meeting, AIAA Paper 92-3638, 1992.
[12] R. Gaffney, J. White, S. Girimaji, J. Drummond, Modeling temperature and species fluctuations in turbulent reacting flow, Comput. Syst. Eng. 5 (2) (1994) 117–133.
[13] A. Beretta, N. Mancini, F. Podenzani, L. Vigevano, The influence of the temperature fluctuations variance on no predictions for a gas flame, Combust. Sci. Tech. 121 (1996) 193–216.
[14] M. Martin, G. Candler, Temperature fluctuation scaling in reacting boundary layers, in: Annual Research Briefs-2001, Center for Turbulence Research, NASA AMS/Standford University, USA, 2001, pp. 151–162.
[15] D. Lee, C. Rutland, Probability density function combustion modeling of a diesel engines, Combust. Sci. Tech. 174 (10) (2002) 19–54.
[16] P. Gerlinger, Investigation of an assumed pdf approach for finite-rate chemistry, Combust. Sci. Tech. 175 (5) (2003) 841–872.
[17] M. Martin, G. Candler, Effect of chemical reactions on decaying isotropic turbulence, Phys. Fluids 10 (1998) 1715–1724.
[18] M. Martin, G. Candler, Subgrid-scale model for temperature fluctuations in reacting hypersonic turbulent flows, Phys. Fluids 11 (1999) 2765–2771.
[19] S. Pope, Consistent modeling of scalars in turbulent flows, Phys. Fluids 26 (1983) 404–408.
[20] M. Chung, H. Sung, Four-equation turbulence model for prediction of the turbulent boundary layer affected by buoyancy force over a flat plate, Int. J. Heat Mass Transfer 27 (12) (1984) 2387–2395.
[21] J. Kim, P. Moin, R. Moser, Turbulence statistics in fully developed channel flow at low Reynolds number, J. Fluid Mech. 177 (1987) 133–166.
[22] Y. Nagano, C. Kim, A two-equation model for heat transport in wall turbulent shear flows, J. Heat Transfer 110 (1988) 583–589.
[23] N. Kasagi, Y. Tomita, A. Kuroda, Direct numerical simulation of passive scalar field in a turbulent channel flow, Trans. ASME, J. Heat Transfer 114 (1992) 598–606.
[24] Y. Lai, R. So, Near-wall modeling of turbulent heat fluxes, Int. J. Heat Mass Transfer 33 (7) (1990) 1429–1440.
[25] T. Sommer, R. So, Y. Lai, A near-wall two-equation model for turbulent heat fluxes, Int. J. Heat Mass Transfer 35 (1992) 3375–3387.
[26] R. So, T. Sommer, A near-wall eddy conductivity model for fluids with different Prandtl numbers, J. Heat Transfer 116 (1994) 844–855.

[27] H. Hattori, Y. Nagano, Rigorous modeling of temperature variance and its dissipation-rate equations using DNS databases, in: Proceedings of the Fourth ASME–JSME Thermal Engineering Joint Conference, vol. 1, 1995, pp. 401–408.
[28] M. Karcz, J. Badur, An alternative two-equation turbulent heat diffusivity closure, Int. J. Heat Mass Transfer 48 (2005) 2013–2022.
[29] S. de Bruyn Kops, J. Riley, Re-examining the thermal mixing layer with numerical simulations, Phys. Fluids 12 (1) (2000) 185–192.
[30] Z. Guo, H. Zhang, C. Chan, W. Lin, Presumed joint probability density function model for turbulent combustion, Fuel 82 (9) (2003) 1091–1101.
[31] R. Baurle, S. Girimaji, Assumed pdf turbulence-chemistry closure with temperature-composition correlations, Combust. Flame 134 (2003) 131–148.
[32] O. Colin, A. Benkenida, C. Angelberger, 3D modeling of mixing, ignition and combustion phenomena in highly stratified gasoline engines, Oil Gas Sci. Technol. 58 (1) (2003) 47–62.
[33] D. Donzis, K. Sreenivasan, P. Yeung, Scalar dissipation rate and dissipative anomaly in isotropic turbulence, J. Fluid Mech. 532 (2005) 199–216.
[34] J. Chang, Z. Filip, D. Assanis, T.-W. Kuo, P. Najt, R. Rask, New heat transfer correlation for the HCCI engine derived from measurements of instantaneous surface heat flux, in: Proceedings of the Powertrain and Fluid Systems Conference and Exhibition, SAE Technical Paper 2004-01-2996, Tempa, Florida, USA, 2004.
[35] U. Piomelli, S. Radhakrishnan, L. Zhong, M. Li, Wall-layer models for large-eddy simulations of high reynolds number non-equilibrium flow, in: J.M.L.M. Palma, A.S. Lopes (Eds.), Proceedings of the 11th EUROMECH European Turbulence Conference, Advances in Turbulence XI, Springer-Verlag, 2007, p. 47.
[36] T. Poinsot, D. Veynante, Theoretical and Numerical Combustion, second ed., R.T. Edwards, 2005.
[37] J. Vogel, J. Eaton, Combined heat transfer and fluid dynamic measurements of a backward facing step, J. Heat Transfer 107 (1985) 922–929.
[38] W. Kays, M. Crawford, Convective Heat and Mass Transfer, third ed., McGraw Hill, New York, 1994.
[39] Z. Han, R. Reitz, F. Corcione, G. Valentino, Interpretation of $k-\epsilon$ computed turbulence length scale predictions for engine flows, in: 26th Symposium (Int) on Combustion, The Combustion Institute, Pittsburgh, 1996, pp. 2717–2723.
[40] C. Angelberger, T. Poinsot, B. Delhaye, Improving near-wall combustion and wall heat transfer modelling in si engine computations, in: Proceedings of the Int. Fall Fuels and Lub. Meeting and Exposition, SAE Technical Paper 972881, 1997.
[41] M. Zolver, D. Klahr, J. Bohbot, O. Laget, A. Torres, Reactive CFD in engines with a new unstructured parallel solver, Oil Gas Sci. Technol. 58 (1) (2003) 33–46.
[42] B. Reveille, S. Henriot, O. Laget, A. Kleemann, S. Jay, Gasoline engine development using CFD, in: Proceedings of the Powertrain and Fluid Systems Conference and Exhibition, SAE Technical Paper 2005-01-3814, San Antonio, Texas, USA, 2005.
[43] B. Launder, Kolmogorov's two-equation model of turbulence, in: Proceedings of the Roy. Soc. London Ser. A., vol. 434, 1991, pp. 214–214.
[44] E. Bahraoui, Contribution à l'étude d'un écoulement turbulent en présence de combustion, Ph.D. thesis, IMST, Marseille, France, 1981.
[45] E. Bahraoui, D.J.G. Brun, L. Fulachier, Experimental and numerical study of a heated turbulent round jet, in: C.-M. Brauner, C. Schmidt-Lainé (Eds.), Modeling in Combust. and Related Topics, 1988, pp. 365–373.
[46] H. Kong, H. Choi, J. Lee, Direct numerical simulation of turbulent thermal boundary layers, Phys. Fluids 12 (10) (2000) 2555–2568.
[47] M. Hishida, Y. Nagano, Structure of turbulent velocity and temperature fluctuations in fully developed pipe flow, Trans. ASME, J. Heat Transfer 101 (1979) 15–22.
[48] Y. Nagano, M. Hishida, Production and dissipation of turbulent velocity and temperature fluctuations in fully developed pipe, in: Proceedings of the Fifth Symposium on Turb. Shear Flow, Cornell University, Ithaca, New York, 1985, pp. 14.19–14.24.
[49] Y. Nagano, H. Sato, M. Tagawa, Structure of heat transfer in the thermal layer growing in a fully developed turbulent flow, Turbulent Shear Flows, vol. 9, Springer-Verlag, Berlin Heidelberg, 1995, p. 364.
[50] Y. Nagano, M. Tagawa, Statistical characteristics of wall turbulence with a passive scalar, J. Fluid Mech. 196 (1988) 157–185.
[51] Z. Warhaft, J. Lumley, An experimental study of decay of temperature fluctuation in grid-generated turbulence, J. Fluid Mech. 88 (1978) 659–684.
[52] A. Sirivat, Z. Warhaft, The effect of a passive cross-stream temperature gradient on the evolution of temperature variance and heat flux in grid turbulence, J. Fluid Mech. 128 (1982) 323–346.
[53] C. Béguier, I. Dekeyser, B. Launder, Ratio of scalar and velocity dissipation times scales in shear flow turbulence, Phys. Fluids 21 (3) (1978) 307–310.
[54] C. Angelberger, Contribution à la modélisation de l'interaction flamme-paroi et des flux pariétaux dans les moteurs à allumage commandé, Ph.D. thesis, INP, Toulouse, France, 1997.
[55] C. Chieng, B. Launder, On the calculation of turbulent heat transport downstream from an abrupt pipe expansion, Numer. Heat Transfer 3 (1980) 189–207.
[56] N. Kasagi, O. Iida, Progress in direct numerical simulation of turbulent heat transfer, in: Proceedings of the Fifth ASME–JSME Joint Thermal Eng. Conf., AJTE99-6302, San Diego, California, USA, 1999.
[57] H. Kawamura, H. Abe, Y. Matsuo, DNS of turbulent heat transfer in channel flow with respect to Reynolds and Prandtl number effects, Int. J. Heat Fluid Flow 20 (1999) 196–207.
[58] Y. Seki, H. Abe, H. Kawamura, DNS of turbulent heat transfer in a channel flow with different thermal boundary conditions, in: Proceedings of the 6th ASME–JSME Joint Thermal Eng. Conf., TED-AJ03-226, Hawaii, USA, 2003.
[59] E. Dahlhaus, Efficient parallel and linear time split decomposition, in: P. Thiagarajan (Ed.), 14th FST-TCS, vol. 34, Springer-Verlag, Berlin, Heidelberg, 1994, pp. 171–180.
[60] E. Mayer, D. Divoky, Correlation of intermittency with preferential transport of heat and chemical species in turbulent shear flows, AIAA J. 4 (1966) 1995–2000.
[61] B. Launder, Heat and mass transport, in: P. Bradshaw (Ed.), Turbulence, Topics in Applied Physics, vol. 12, Springer-Verlag, Berlin, Heidelberg, 1976, pp. 231–287.
[62] A. Chambers, R. Antonia, L. Fulachier, Turbulent Prandtl number and spectral characteristic of a turbulent mixing layer, Int. J. Heat Mass Transfer 28 (1985) 1461–1468.
[63] F. Nicoud, T. Poinsot, DNS of a channel flow with variable properties, in: S. Banerjee, J. Eaton (Eds.), First International Symposium on Turb. and Shear Flow Phenomena, Santa Barbara, USA, 1999, p. 697.
[64] H. Kawamura, H. Abe, K. Shingai, DNS of turbulent heat transfer in channel flow with different Reynolds and Prandtl numbers and boundary conditions, in: Y. Nagano et al. (Eds.), Proceedings of the Third International Symposium Turb., Heat and Mass Transfer, Nagoya, Japan, 2000, pp. 15–32.
[65] B. Debusschere, C. Rutland, Turbulent scalar transport mechanisms in plane channel and Couette flows, Int. J. Heat Mass Transfer 47 (2004) 1171–1181.
[66] A. Perry, P. Hoffmann, An experimental study of turbulent convective heat transfer from a plate, J. Fluid Mech. 77 (1976) 355–368.
[67] R. Cheng, T. Ng, Some aspects of strongly heated turbulent boundary layer flow, Phys. Fluids 25 (8) (1982) 1333–1341.
[68] M. Karcz, J. Badur, A turbulent heat flux two-equation turbulent $\overline{\theta'^2}-\epsilon_\theta$ closure based on the V2F turbulence model, Task Quart. 7 (3) (2005) 375–387.
[69] J. Dec, W. Hwang, M. Sjöberg, An investigation of thermal stratification in HCCI engines using chemiluminescence imaging, in: Proceedings of the SAE World Congress and Exhibition, SAE Technical Paper 2006-01-1518, Detroit, Michigan, USA, 2006.